RSC Advances

PAPER

View Article Online
View Journal | View Issue

Cite this: *RSC Adv.*, 2021, **11**, 29065

NIR-triggered upconversion nanoparticles@thermo-sensitive liposome hybrid theranostic nanoplatform for controlled drug delivery†

Yibin Yu,[af] Yida Huang,[b] Wanqian Feng,[c] Mei Yang,[b] Baiqi Shao, *[af] Jingjing Li*[d] and Fangfu Ye *[aef]

Posterior segment ocular diseases are highly prevalent worldwide due to the lack of suitable noninvasive diagnostic and therapeutic tactics. Herein, concerning this predicament, we designed a hybrid retina-targeted photothermal theranostic nanoplatform (UCNPs@Bi@SiO_2@GE HP-lips), based on the unique upconversion luminescence (UCL) imaging of upconversion nanoparticles (UCNPs), efficient photothermal conversion ability of Bi nanoparticles, and thermal-induced phase transition properties of the liposomes (lips). The nanoplatform was functionalized with penetratin (PNT) and hyaluronic acid (HA), to obtain retina-targeted liposomes (HP-lips). Lipophilic genistein (GE) was entrapped into the liposomes (GE HP-lips). An *in vitro* release study showed NIR irradiation could photothermally trigger controlled release of GE from the liposomal platform. Moreover, cellular uptake evaluation *via* UCL imaging demonstrated UCNPs@Bi@SiO_2@GE HP-lips represented the brightest UCL, compared with other formulations, which is beneficial for the accurate evaluation of the prognosis and severity of angiogenesis-related posterior segment disorders. Therefore, UCNPs@Bi@SiO_2@GE HP-lips exhibit promising potential as a theranostic nanoplatform for posterior segment ocular diseases.

Received 8th June 2021
Accepted 5th August 2021

DOI: 10.1039/d1ra04431a

rsc.li/rsc-advances

Posterior segment ocular diseases, such as age-related macular degeneration (AMD) and diabetic retinopathy (DR), have drawn considerable attention worldwide. Both AMD and DR are highly prevalent and have been proven to be the leading causes of blindness in the developed nations, resulting in a heavy social burden.[1,2] It is common sense that neovascularization in the posterior segment, including choroidal neovascularization (CNV) and retinal neovascularization (RNV), is the primary cause of severe visual impairment.[3] Research has shown that suitable therapeutic tactics, as well as timely and precise diagnostic avenues, are highly crucial to the prevention and/or treatment of angiogenesis-related ocular disorders. Therefore, it is high time to develop proper platforms with desirable diagnostic and therapeutic abilities for angiogenesis-related ocular disorders.

For accurate evaluation of the prognosis and severity of angiogenesis-related posterior segment disorders, convenient and efficient imaging techniques of angiogenesis are the prerequisites. Diverse nanoprobes for bioimaging are one of the best fruits of the quick development of nanotechnology.[4–7] Many organic imaging agents have been employed in the field of bioimaging.[8–10] Besides organic bioimaging agents, inorganic lanthanide (Ln^{3+})-doped upconversion nanoparticles (UCNPs), which can convert low-energy NIR light into higher-energy UV/visible/NIR light, have attractive superiorities over conventional organic dyes and quantum dots, such as high signal-to-noise ratio, low auto-fluorescence background, narrow emission peak width, superb stability, and absence of photodamage to live organisms.[7,11,12] Accordingly, UCNPs have been broadly investigated as emerging luminescent nanoprobes for real-time bioimaging and drug release tracking in recent decades.[13,14] Especially, NIR light shows an adequate penetration depth in deep tissue, which promotes *in vivo* bioimaging application of UCNPs.[15] Additionally, UCNPs have been widely employed as a building block to construct multimodal imaging nanoplatforms to enhance their imaging precision or equipped with

[a]*Wenzhou Institute, University of the Chinese Academy of Sciences, Wenzhou 325001, China. E-mail: bqshao@ciac.ac.cn*

[b]*Institute of Advanced Materials for Nano-bio Applications, Wenzhou Medical University, Wenzhou 325027, China*

[c]*Scientific Research Center, Wenzhou Medical University, Wenzhou 325035, China*

[d]*State Key Laboratory of Rare Earth Resource Utilization, Changchun Institute of Applied Chemistry, Chinese Academy of Sciences, Changchun 130022, China. E-mail: jjingli@ciac.ac.cn*

[e]*Beijing National Laboratory for Condensed Matter Physics, Institute of Physics, Chinese Academy of Sciences, Beijing 100190, China. E-mail: fye@iphy.ac.cn*

[f]*Oujiang Laboratory (Zhejiang Lab for Regenerative Medicine, Vision and Brain Health), Wenzhou, Zhejiang 325001, China*

† Electronic supplementary information (ESI) available. See DOI: 10.1039/d1ra04431a

therapeutic functionality by surface functionalization, designing hierarchical nanostructures with other functional nanoparticles and introducing diversiform doped ions.[16,17] Rieffel *et al.* have designed porphyrin–phospholipid-coated UCNPs, realizing at least six imaging modalities, including upconversion luminescence imaging, fluorescence imaging, positron emission tomography, computed tomography, photoacoustic imaging, and Cerenkov luminescence imaging.[18] To integrate the photothermal function into UCNPs, diverse UCNPs-based nanocomposites with different nanostructure have been developed, such as UCNPs-Au,[19] UCNPs-CuS,[20] UCNPs-Cu_2S,[21] UCNPs-Ag_2S,[22] and UCNPs-Bi_2Se_3.[16] These nanocomposites structurally combining UCNPs with photothermal agents would not only achieve real-time monitoring of *in vivo* agent distribution, but can also endow UCNPs with photothermal therapeutic ability. Numerous studies of UCNPs-based nanoplatforms for diagnosis and therapy of tumors present an undeniable interest in the biomedical application of UCNPs.[5,23–25] Very recently, UCNPs have been utilized in the field of ophthalmic application. Ma *et al.* designed retinal photoreceptor-binding upconversion nanoparticles (pbUCNPs) and endowed the mice with NIR light image vision while their normal vision and related behavioral responses were not compromised.[26] Microenvironment-triggered degradable hydrogels were designed by Li *et al.* using ultrasmall UCNPs, and exhibited its potential application in non-invasive NIR-II imaging diagnosis and combined therapy in human choroidal melanoma.[27]

Current therapeutic strategies of angiogenesis-related ocular disorders are far from satisfactory. It is universally acknowledged that intraocular injection of anti-vascular endothelial growth factor (VEGF) agents has been broadly accepted as a "gold standard" treatment for angiogenesis-related ocular diseases and in a way, can ameliorate the visual impairment of DR and AMD patients.[28] Nonetheless, repeated invasive injections enhance the risk of complications, compromise patient compliance, and aggravate the burden of healthcare.[29] Topical instillation of eye drops is the most common and accessible route to treat ocular diseases due to its convenient and painless properties, however, multiple ocular barriers (including cornea, conjunctiva, sclera, blood-retinal barrier, and blood-aqueous barrier) result in a negligible permeated amount of drug to the posterior segment by topical administration.[2] Recently, photo-driven therapy, such as photodynamic therapy (PDT) and photothermal therapy (PTT), have been widely used in biomedicine and many organic components play key roles.[30,31] Additionally, light has been widely employed as a non-invasive external stimulus for remote spatiotemporal controlled drug release.[7,32] Light-triggered drug delivery platforms exhibit attractive advantages, including low cost, outstanding therapeutic effect and little damage to physiological tissue, and hence are suitable for non-invasive ocular drug delivery, in terms of intrinsic anatomical and biological constraints of eyes. It is reported that cell penetrating peptides (CPPs), which can promote the transport of various cargos across the cell membrane, have evoked considerable interest in pharmaceutical applications.[33,34] Among the peptides, penetratin (PNT), a cationic and amphipathic CPP, was demonstrated to have excellent penetration through multiple physiological barriers in the eyes, promoting drug transport to the posterior segment.[35,36] Angiogenesis-related posterior segment diseases can result in the overexpression of cluster of differentiation 44 (CD44) in the retina.[37,38] As we all know, hyaluronic acid (HA) is a specific ligand of the CD44 receptor. Accordingly, HA can be applied as a retina-targeted ligand for posterior ocular drug delivery. In short, PNT and HA are ideal constituent parts to design retina-targeted theranostic nanoplatforms towards diagnosis and therapy for angiogenesis-related posterior ocular diseases.

Herein, we designed a hybrid photothermal stimuli-responsive theranostic nanoplatform, UCNPs@Bi@SiO_2@GE

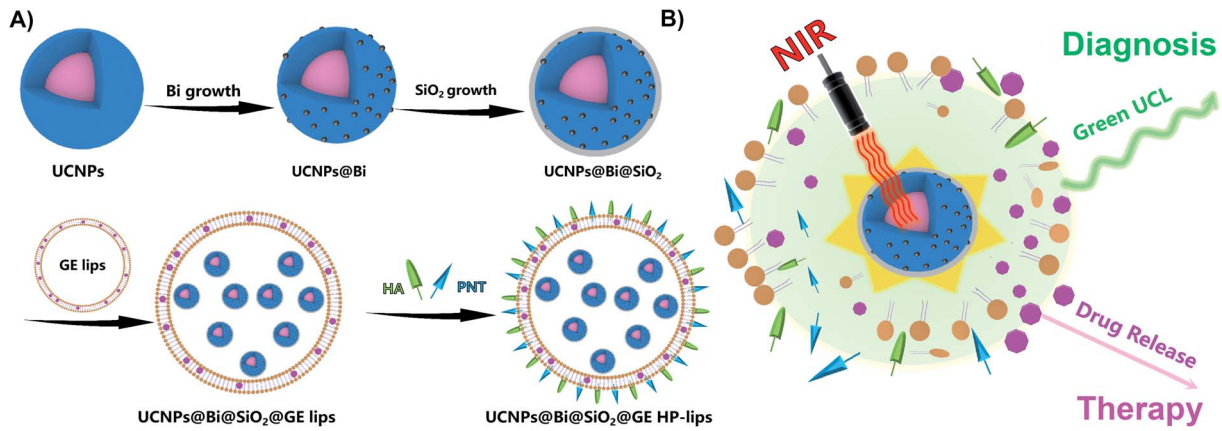

Fig. 1 Schematic diagram of UCNPs@Bi@SiO_2@GE HP-lips for NIR-triggered drug release. (A) The fabrication procedure of UCNPs@Bi@SiO_2@GE HP-lips. As proposed, hydrophilic UCNPs@Bi@SiO_2 and lipophilic drug GE were loaded in the aqueous core and lipid bilayer of the liposome frameworks, respectively. Cell penetrating peptide PNT and retina-targeted ligand HA were conjugated by amidation reaction in the preformed liposome bilayer. (B) Upon NIR irradiation, UCNPs@Bi@SiO_2 in the aqueous core of the liposomal platform could generate mild heat, which realized real-time green UCL monitoring and photothermally triggered drug release.

HP-lips with the retina-targeted ability (Fig. 1), to realize the combined diagnosis and therapy for angiogenesis-related posterior diseases. Genistein (GE), an anti-angiogenic agent that could suppress CNV formation, was selected as the model drug.[39] *In vitro* release study revealed UCNPs@Bi@SiO_2 in the aqueous core of the liposomal platform could generate mild heat upon NIR irradiation, which facilitated phase transition of thermo-sensitive phospholipid DPPC, enhanced the fluidity of lipid layer, and hence triggered the release of GE from the liposomal platform. The admirable cytocompatibility of the nanocomposites with ARPE-19 cells was demonstrated by CCK-8 assay and live/dead cell staining. Moreover, UCL imaging proved cellular uptake of the nanocomposites by ARPE-19 cells was time-dependent and UCNPs@Bi@SiO_2@HP-lips showed the brightest UCL, compared with other formulations. Therefore, UCNPs@Bi@SiO_2@GE HP-lips could be a potential theranostic nanoplatform for posterior segment diseases.

Results and discussion

Upconversion nanoparticles (UCNPs) are the emerging luminescent nanoprobes for real-time bioimaging and drug release tracking. In this theranostic nanoplatform, β-$NaYF_4$: 20% Yb, 2% Er UCNPs were employed as the UCL probe. As observed by the TEM image (Fig. 2A), UCNPs presented a hexagonal structure with a uniform size of about 30 nm. The characteristic UCL spectra of UCNPs were acquired upon a 980 nm laser irradiation. As represented in Fig. S1,† the sensitizer Yb^{3+} transferred energy to the activator Er^{3+}, and hence generated the multiple UCL emission bands at 524, 542 and 655 nm. For further study, hydrophilic ligand-free UCNPs were acquired through the removal of oleate ligand from hydrophobic oleic acid

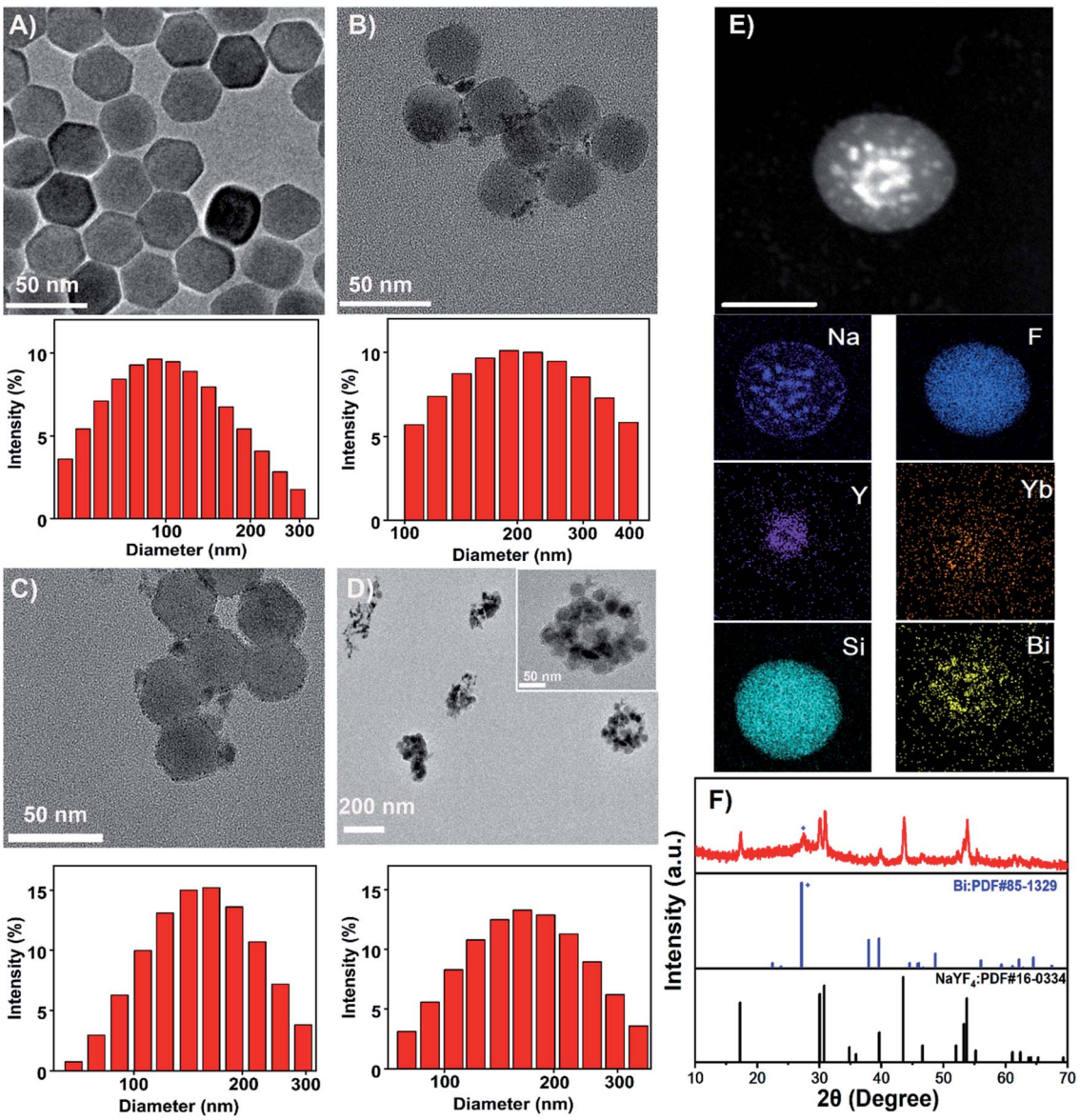

Fig. 2 TEM images and DLS particle size distribution of (A) UCNPs, (B) UCNPs@Bi, (C) UCNPs@Bi@SiO_2, (D) UCNPs@Bi@SiO_2 lips. (E) Element mapping of UCNPs@Bi@SiO_2. Scale bars in figure (A), (B), (C), (E), and inset in (D) are 50 nm. (F) XRD patterns of UCNPs@Bi@SiO_2.

(OA)-capped UCNPs, and could be proved by FTIR (Fig. S2†). OA-capped UCNPs presented its characteristic band at 2924 cm^{-1}, ascribed to the existence of =CH stretching. The band at 667 cm^{-1} could be attributed to the bending vibration of =CH. Two peaks at 1631 and 1561 cm^{-1} could be characteristics of the asymmetrical and the symmetrical stretching vibrations of COO−, separately. UCNPs@Bi and UCNPs@Bi@SiO_2 were fabricated as reported earlier by our group.[40] Photothermal agent Bi nanoparticles were epitaxially grown onto hydrophilic UCNPs, as showed in Fig. 2B, and one could see that Bi nanoparticles formed on the surface of hydrophilic UCNPs. A SiO_2 layer was coated onto UCNPs@Bi nanocomposites to elevate the stability and protected the Bi nanoparticles from oxidation. The wall thickness of the SiO_2 layer was about 2 nm, while the average particle size of UCNPs@Bi@SiO_2 was approximately 50 nm. Moreover, Si, Bi, and rare earth (Y and Yb) elements were clearly detected by high-angle annular dark-field scanning TEM-energy dispersive X-ray spectroscopy (HAADF-STEM-EDS) analysis (Fig. 2E), further proving the successful fabrication of UCNPs@Bi@SiO_2. XRD measurements were performed to investigate the crystalline information and impurity profile of UCNPs@Bi@SiO_2. As represented in Fig. 2F, a diffraction peak at $2\theta = 20.23°$ was observed in the pattern of UCNPs@Bi@SiO_2, which could be ascribed to the (012) planes of Bi (JCPDS no. 85-1329). Other peaks could be due to the hexagonal phase of $NaYF_4$ (JCPDS no. 16-0334). It is difficult to find SiO_2 by XRD because of its amorphous structure, while there was no other obvious peak in the pattern of UCNPs@Bi@SiO_2, which indicated there was negligible impurity of UCNPs@Bi@SiO_2 production. In liposomal frameworks, aqueous core and lipid bilayer can load hydrophilic and lipophilic cargos, separately. Herein, hydrophilic UCNPs@Bi@SiO_2 was encapsulated into the biocompatible liposomes by thin film hydration combined with extrusion technique. As represented in Fig. 2D, we could clearly observe that several UCNPs@Bi@SiO_2 nanocomposites were loaded into a liposomal particle and the UCNPs@Bi@SiO_2 lips presented a mean hydrodynamic size of about 150 nm. Meanwhile, the mean hydrodynamic size of UCNPs@Bi@SiO_2 lips was 151.2 ± 1.5 nm, in agreement with the results of TEM. In order to endow the nanoplatform with the retina-targeted ability, hyaluronic acid (HA) and penetratin (PNT) were conjugated onto the surface of the liposomes. HA density on the UCNPs@Bi@SiO_2 HP-lips surface was estimated by CTAB turbidometric assay. Around 138.7 ± 3.4 μg of HA was conjugated per mg of the liposomes. PNT density on the UCNPs@Bi@SiO_2 HP-lips surface of the liposomes was estimated using a BCA protein assay kit, around 5.9 ± 0.8 μg mg^{-1} of the liposomes. Therefore, the hybrid theranostic nanoplatform based on UCNPs@Bi@SiO_2 and thermo-sensitive liposomes with retina-targeted ability had been successfully fabricated.

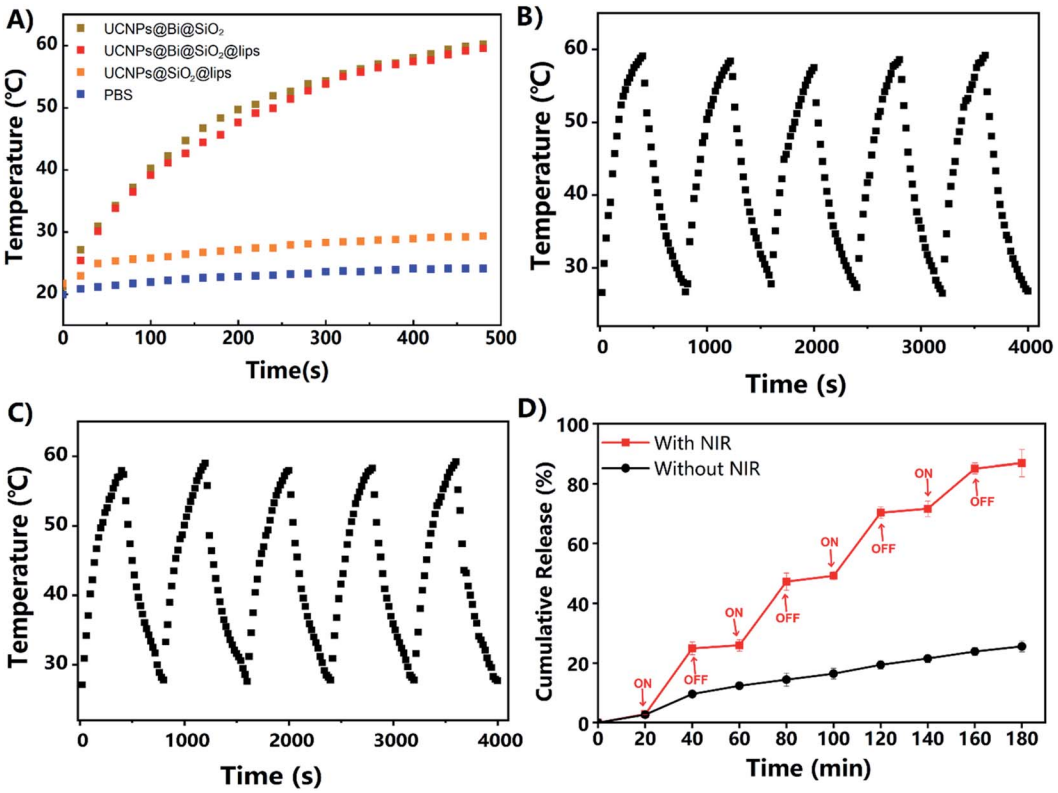

Fig. 3 (A) Photothermal conversion profiles of PBS, UCNPs@Bi@SiO_2, and UCNPs@Bi@SiO_2 lips upon CW NIR laser exposure (808 nm, 500 mW cm^{-2}). (B) Photothermal conversion profiles of UCNPs@Bi@SiO_2 over 5 cycles of NIR on/off. (C) Photothermal conversion profiles of UCNPs@Bi@SiO_2 lips over 5 cycles of NIR on/off. (D) *In vitro* GE release profiles from UCNPs@Bi@SiO_2@GE HP-lips with/without intermittent NIR exposure. Red-marked pattern indicated the release of GE from UCNPs@Bi@SiO_2@GE HP-lips under periodically controlled on/off of CW NIR laser exposure and every duration of NIR irradiation is 20 min. Black-marked pattern indicated the release of GE from UCNPs@Bi@SiO_2@GE HP-lips without CW NIR laser exposure.

The photothermal features of UCNPs@Bi@SiO_2 and UCNPs@Bi@SiO_2 lips were investigated upon a CW NIR laser excitation (808 nm, 500 mW cm^{-2}). As exhibited in Fig. 3A, the photothermal conversion profiles of UCNPs@Bi@SiO_2 and UCNPs@Bi@SiO_2 lips were similar, suggesting the liposomes coating and drug loading had negligible effects on the photothermal conversion capacity of UCNPs@Bi@SiO_2. Especially, the temperature of UCNPs@Bi@SiO_2 lips rise from 21.2 °C to 49.9 °C within 4 min during NIR irradiation process, meanwhile, the increment of temperature was only 2.9 °C for PBS at the same period. Therefore, UCNPs@Bi@SiO_2 lips could convert NIR into controllable heat in a time-dependent way. Additionally, IR thermal photos taken by the thermal imager (Fig. S4†) were consistent with the temperature records by a thermocouple microprobe, which demonstrated the desirable photothermal conversion efficiency of UCNPs@Bi@SiO_2 was inherited by UCNPs@Bi@SiO_2 lips. Concurrently, the photothermal stability of UCNPs@Bi@SiO_2 lips was evaluated by heating–cooling cycles assay. As represented in Fig. 3B and C, UCNPs@Bi@SiO_2 and UCNPs@Bi@SiO_2 lips consistently caused controllable increment of temperature during 5 cycles, attributed to photothermal Bi nanoparticles under the protection of SiO_2 shell. The results suggested that UCNPs@Bi@SiO_2 lips represented desirable photothermal conversion features and photothermal stability.

Lipophilic drug genistein was encapsulated into the lipid bilayer of the UCNPs@Bi@SiO_2 lips. Entrapment efficiency (EE, %) and drug loading (DL, %) were quantified by HPLC. As represented in Table S1,† EE and DL of UCNPs@Bi@SiO_2@GE HP-lips were 80.26 ± 1.92% and 5.23 ± 0.32%, exhibited no significant differences from those of GE lips ($p > 0.05$). The results reflected that the incorporation of hydrophilic nanocomposites and surface functionalization could not reduce the encapsulation ability of the liposomes for hydrophobic drugs. UCNPs@Bi@SiO_2@GE HP-lips could keep stable for 7 days, as presented in Fig. S4.† Photothermally triggered drug release of UCNPs@Bi@SiO_2@GE HP-lips was investigated upon intermittent NIR irradiation, so as to obviate overheating of the released medium.[41] The release profile of UCNPs@Bi@SiO_2@GE HP-lips under light exclusion was also investigated, as the control group. The cumulative amount of genistein released from UCNPs@Bi@SiO_2@GE HP-lips upon intermittent NIR exposure was 86.9 ± 4.5% within 3 h, while that from UCNPs@Bi@SiO_2@GE HP-lips in the control group was only 25.6 ± 1.8% after 3 h. Furthermore, it is a "stepped" drug release pattern that UCNPs@Bi@SiO_2@GE HP-lips upon intermittent NIR exposure represented: drug release accelerated with NIR and could be slowed down when NIR light was off. Accordingly, the release of genistein could be controlled by NIR laser, which could be ascribed to the NIR-triggered heat that potentially destructed the lipid bilayer containing thermosensitive phospholipid DPPC. In addition, the cumulative amount of genistein released from GE HP-lips without UCNPs@Bi@SiO_2 was only 30.8 ± 1.2% upon intermittent NIR exposure within 4 h, as represented in Fig. S5,† revealing that UCNPs@Bi@SiO_2 was necessary for NIR-triggered controlled drug release. Above results suggested UCNPs@Bi@SiO_2@GE HP-lips is an appropriate platform for photothermally triggered controlled release of the hydrophobic drug.

An ocular drug delivery platform must have little toxicity to eye tissue.[42] In the present study, the cytocompatibility of various formulations with ARPE-19 cells was assessed by CCK-8 assay and calcein-AM/PI staining. The viability of ARPE-19 cells was measured, as represented in Fig. 4A and S6–S10.† The negative control group was treated by the culture medium without any sample. There was no cytotoxicity against ARPE-19 cells in blank lips, blank HP-lips, and GE lips groups, indicating these liposomal formulations are cytocompatible. Nonetheless, the UCNPs group represented unsatisfactory cytocompatibility with ARPE-19 cells, which was perhaps due to intrinsic low

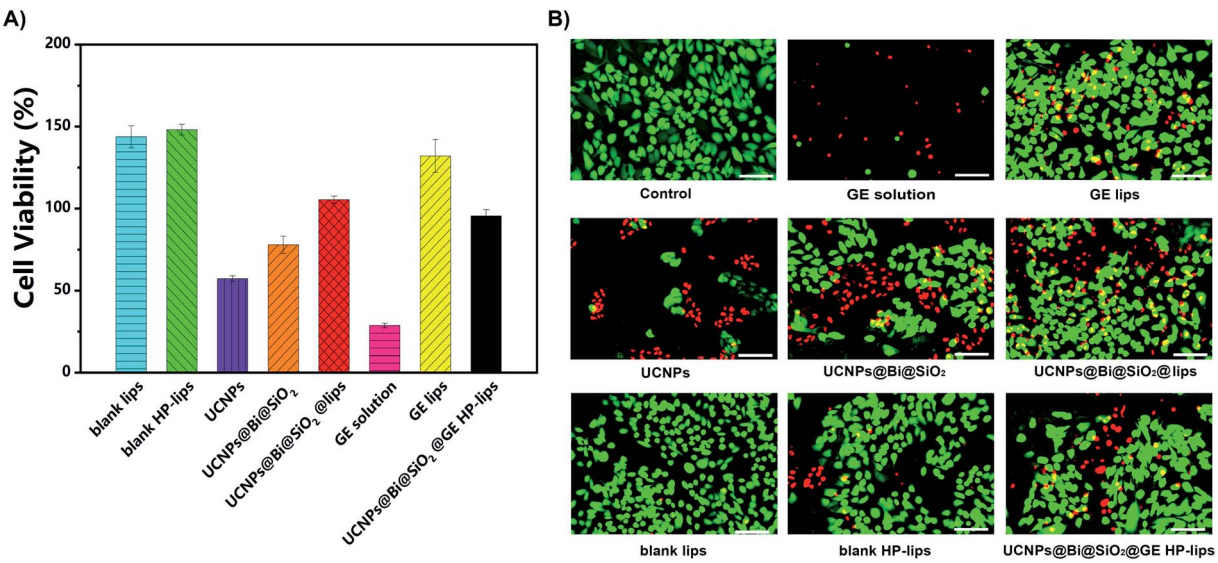

Fig. 4 Cytocompatibility of various formulations with ARPE-19 cells for 24 h. (A) CCK-8 assay ($n = 6$), (B) images of calcein-AM/PI staining. The control group was treated by the culture medium without any sample. Scale bars: 100 μm.

biocompatibility of lanthanide (Ln^{3+})-doped UCNPs. The viability of ARPE-19 cells was enhanced after the silanization of UCNPs, and the incorporation into the biocompatible liposomes could further improve the cytocompatibility of the nanocomposites. Additionally, the viability of ARPE-19 cells in the GE solution group was the lowest. In the present study, DMSO was utilized as the solvent to dissolve the lipophilic genistein. Although DMSO is an efficacious penetration enhancer, residual DMSO could change the penetrability of the cell membrane and hence few living ARPE-19 cells after being treated with UCNPs, while more living ARPE-19 cells in the groups of UCNPs@Bi@SiO_2, UCNPs@Bi@SiO_2 lips, and UCNPs@Bi@SiO_2@GE HP-lips. Most ARPE-19 cells in other groups were alive, which was in accordance with the results of the CCK-8 assay. Above results suggested UCNPs@Bi@SiO_2@-GE HP-lips was a safe ophthalmic platform and had excellent cytocompatibility with ARPE-19 cells.

Cellular uptake and distribution of various upconversion nanocomposites in APRE-19 cells were monitored by a multiphoton laser scanning microscope. Blue fluorescence signal of DAPI depicted the cell nuclei, and green UCL signal illustrated that the cellular distribution of different upconversion nanocomposites. In merged channel, green UCL signal overlapped the blue fluorescence of DAPI, represented as cyan. The luminescence photos of ARPE-19 cells upon 980 nm NIR laser exposure co-cultured with distinct formulations for 24 h were represented in Fig. 5. As exhibited in Fig. 5, green UCL signal could be observed in all groups, which revealed UCNPs, UCNPs@Bi@SiO_2, UCNPs@Bi@SiO_2 lips, and UCNPs@Bi@SiO_2@HP-lips could be internalized by ARPE-19 cells, while well-distinguished signal intensity differences of

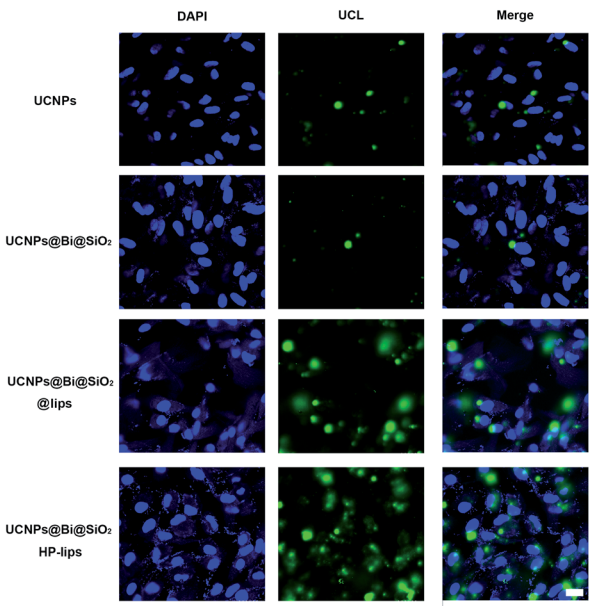

Fig. 5 Multiphoton laser scanning microscopy observation of ARPE-19 cells upon 980 nm NIR laser exposure incubated with UCNPs, UCNPs@Bi@SiO_2, UCNPs@Bi@SiO_2, and UCNPs@Bi@SiO_2@HP-lips for 24 h, respectively. Scale bar: 20 μm.

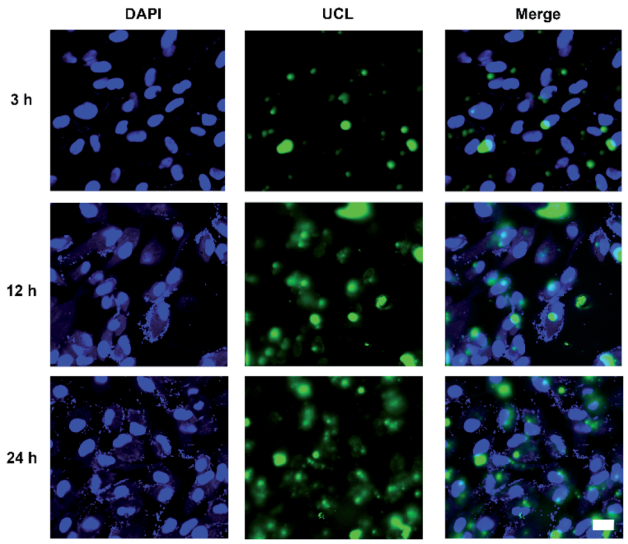

Fig. 6 Multiphoton laser scanning microscopy observation of ARPE-19 cells upon 980 nm NIR laser exposure incubated with UCNPs@Bi@SiO_2@HP-lips for 3 h, 12 h, and 24 h. Scale bars are 20 μm.

green UCL suggested cellular uptake amounts of the nanocomposites were apparently different. Green UCL signal in UCNPs@Bi@SiO_2 group was weaker than that in UCNPs group, perhaps owing to the quenching effect of silica coating.[43] Nonetheless, UCNPs@Bi@SiO_2 lips represented a much stronger UCL signal than UCNPs@Bi@SiO_2, which reflected being incorporated into liposome could facilitate the cellular internalization of upconversion nanocomposites, attributed to similar lipid bilayer structure of the liposomes and the cell membrane.[44,45] Moreover, UCNPs@Bi@SiO_2@HP-lips represented the brightest green UCL, thus demonstrating the successful fabrication of retina-targeted nanoplatform. In addition, as represented in Fig. 6, green UCL signals of UCNPs@Bi@SiO_2@HP-lips co-cultured with ARPE-19 cells exhibited an ever-increasing intensity as time progressed, and observed cellular UCL intensity at 24 h was stronger than at 3 h or 12 h. The results suggested that the uptake of UCNPs@Bi@SiO_2@HP-lips by ARPE-19 cells enhanced as the incubation time increased. With desirable UCL imaging and retina-targeted ability, UCNPs@Bi@SiO_2@HP-lips could be employed to visualize the neovascularization for the accurate evaluation of the prognosis and severity of angiogenesis-related posterior segment disorders.

Conclusions

In conclusion, UCNPs@Bi@SiO_2@GE HP-lips, an innovative retina-targeted theranostic nanoplatform for angiogenesis-related posterior segment ocular diseases has been successfully fabricated and characterized. The nanoplatform not only inherited excellent photothermal conversion efficiency of UCNPs@Bi@SiO_2 but also represented admirable cytocompatibility with human retinal pigment epithelial cells, demonstrated by CCK-8 assay and live/dead cell staining. *In vitro*

release study revealed that upon NIR irradiation, UCNPs@Bi@SiO_2@GE HP-lips could generate mild heat, which triggered controlled release of GE from the liposomal platform. Furthermore, cellular uptake evaluation *via* UCL imaging proved that uptake of upconversion nanocomposites by ARPE-19 cells was time-dependent, and compared with other formulations, UCNPs@Bi@SiO_2@HP-lips represented the brightest UCL, suggesting outstanding retina-targeted ability. In short, UCNPs@Bi@SiO_2@HP-lips have promising potential to exhibit combined diagnostic and therapeutic ability for angiogenesis-related posterior ocular diseases. The present proof-of-concept study could afford novel insights into theranostic nanoplatforms for angiogenesis-related posterior segment diseases. Further pharmacokinetic and pharmacodynamic evaluations of UCNPs@Bi@SiO_2@GE HP-lips, are continued to investigate *in vivo* fate and theranostic effect on angiogenesis-related posterior segment diseases of the developed nanoplatform.

Conflicts of interest

There are no conflicts to declare.

Acknowledgements

This work is supported by the National Key Research and Development Program of China (grant no. 2020YFA0908200), the Natural Science Foundation of Jilin Province (Grant No. 20200201106JC) and Wenzhou Institute, University of Chinese Academy of Sciences (Grant No. WIUCASQD2020012). The authors thank the technical support of Scientific Research Center, Wenzhou Medical University, and the Core Facilities, Zhejiang University School of Medicine.

Notes and references

1 Q. Lyu, L. Peng, X. Hong, T. Fan, J. Li, Y. Cui, H. Zhang and J. Zhao, *Biomaterials*, 2021, **270**, 120682.
2 K. Suda, T. Murakami, N. Gotoh, R. Fukuda, Y. Hashida, M. Hashida, A. Tsujikawa and N. Yoshimura, *J. Controlled Release*, 2017, **266**, 301–309.
3 A. Das and P. G. McGuire, *Prog. Retinal Eye Res.*, 2003, **22**, 721–748.
4 J. Shen, L.-D. Sun, J.-D. Zhu, L.-H. Wei, H.-F. Sun and C.-H. Yan, *Adv. Funct. Mater.*, 2010, **20**, 3708–3714.
5 Y. Shao, B. Liu, Z. Di, G. Zhang, L. D. Sun, L. Li and C. H. Yan, *J. Am. Chem. Soc.*, 2020, **142**, 3939–3946.
6 H. Dong, L. D. Sun and C. H. Yan, *Front. Chem.*, 2020, **8**, 619377.
7 D. Yang, P. Ma, Z. Hou, Z. Cheng, C. Li and J. Lin, *Chem. Soc. Rev.*, 2015, **44**, 1416–1448.
8 L. Wu, C. Huang, B. P. Emery, A. C. Sedgwick, S. D. Bull, X. P. He, H. Tian, J. Yoon, J. L. Sessler and T. D. James, *Chem. Soc. Rev.*, 2020, **49**, 5110–5139.
9 H. Cai, X. Dai, X. Wang, P. Tan, L. Gu, Q. Luo, X. Zheng, Z. Li, H. Zhu, H. Zhang, Z. Gu, Q. Gong and K. Luo, *Adv. Sci.*, 2020, **7**, 1903243.
10 S. Onishi, Y. Suzuki, H. Ano and J. Kawamata, *Bull. Chem. Soc. Jpn.*, 2020, **93**, 1226–1233.
11 F. Hu, B. Liu, H. Chu, C. Liu, Z. Li, D. Chen and L. Li, *Nanoscale*, 2019, **11**, 9201–9206.
12 H. Dong, L. D. Sun and C. H. Yan, *Nanoscale*, 2013, **5**, 5703–5714.
13 S. Han, R. Deng, Q. Gu, L. Ni, U. Huynh, J. Zhang, Z. Yi, B. Zhao, H. Tamura, A. Pershin, H. Xu, Z. Huang, S. Ahmad, M. Abdi-Jalebi, A. Sadhanala, M. L. Tang, A. Bakulin, D. Beljonne, X. Liu and A. Rao, *Nature*, 2020, **587**, 594–599.
14 S. Chen, A. Z. Weitemier, X. Zeng, L. M. He, X. Y. Wang, Y. Q. Tao, A. J. Y. Huang, Y. Hashimotodani, M. Kano, H. Iwasaki, L. K. Parajuli, S. Okabe, D. B. L. Teh, A. H. All, I. Tsutsui-Kimura, K. F. Tanaka, X. G. Liu and T. J. McHugh, *Science*, 2018, **359**, 679–683.
15 P. Wang, X. Wang, Q. Luo, Y. Li, X. Lin, L. Fan, Y. Zhang, J. Liu and X. Liu, *Theranostics*, 2019, **9**, 369–380.
16 S. Zhao, R. Tian, B. Shao, Y. Feng, S. Yuan, L. Dong, L. Zhang, Z. Wang and H. You, *Chemistry*, 2020, **26**, 1127–1135.
17 D. Ling, H. Li, W. Xi, Z. Wang, A. Bednarkiewicz, S. T. Dibaba, L. Shi and L. Sun, *J. Mater. Chem. B*, 2020, **8**, 1316–1325.
18 J. Rieffel, F. Chen, J. Kim, G. Chen, W. Shao, S. Shao, U. Chitgupi, R. Hernandez, S. A. Graves, R. J. Nickles, P. N. Prasad, C. Kim, W. Cai and J. F. Lovell, *Adv. Mater.*, 2015, **27**, 1785–1790.
19 B. Liu, J. Sun, J. Zhu, B. Li, C. Ma, X. Gu, K. Liu, H. Zhang, F. Wang, J. Su and Y. Yang, *Adv. Mater.*, 2020, **32**, e2004460.
20 X. Xu, C. Han, C. Zhang, D. Yan, C. Ren and L. Kong, *Theranostics*, 2021, **11**, 6477–6490.
21 G. Xiang, Q. Xia, X. Liu, Y. Wang, S. Jiang, L. Li, X. Zhou, L. Ma, X. Wang and J. Zhang, *Nanoscale*, 2021, **13**, 7161–7168.
22 K. Du, P. Lei, M. Zhang, X. Gao, S. Yao, C. Li, J. Feng and H. Zhang, *Nanoscale*, 2020, **12**, 3977–3987.
23 Y. Wang, S. Song, S. Zhang and H. Zhang, *Nano Today*, 2019, **25**, 38–67.
24 S. Wu and H. J. Butt, *Adv. Mater.*, 2016, **28**, 1208–1226.
25 Y. Lan, X. Zhu, M. Tang, Y. Wu, J. Zhang, J. Liu and Y. Zhang, *Nanoscale*, 2020, **12**, 7875–7887.
26 Y. Ma, J. Bao, Y. Zhang, Z. Li, X. Zhou, C. Wan, L. Huang, Y. Zhao, G. Han and T. Xue, *Cell*, 2019, **177**, 243–255.e15.
27 L. Li, Z. Zeng, Z. Chen, R. Gao, L. Pan, J. Deng, X. Ye, J. Zhang, S. Zhang, C. Mei, J. Yu, Y. Feng, Q. Wang, A. Y. Yu, M. Yang and J. Huang, *ACS Nano*, 2020, **14**, 15403–15416.
28 G. Markus van der, H. Cornelia, S. Mirjam and T. Markus, *Curr. Pharm. Des.*, 2015, **21**, 3548–3556.
29 C. M. L. Lau, Y. Yu, G. Jahanmir and Y. Chau, *Adv. Drug Delivery Rev.*, 2018, **126**, 145–161.
30 L. Li, Y. Liu, T. Sun, T. Zhou, Y. Bai, X. Liu, S. Zhang, T. Jia, X. Zhao and Y. Wang, *J. Mater. Chem. B*, 2021, **9**, 5785–5793.
31 J. Chen, Y. Cui, K. Song, T. Liu, L. Zhou, B. Bao, R. Wang and L. Wang, *Biomater. Sci.*, 2021, **9**, 2115–2123.
32 N. Niu, F. He, P. Ma, S. Gai, G. Yang, F. Qu, Y. Wang, J. Xu and P. Yang, *ACS Appl. Mater. Interfaces*, 2014, **6**, 3250–3262.

33 F. Guo, T. Ouyang, T. Peng, X. Zhang, B. Xie, X. Yang, D. Liang and H. Zhong, *Biomater. Sci.*, 2019, **7**, 1493–1506.
34 S. Pescina, C. Ostacolo, I. M. Gomez-Monterrey, M. Sala, A. Bertamino, F. Sonvico, C. Padula, P. Santi, A. Bianchera and S. Nicoli, *J. Controlled Release*, 2018, **284**, 84–102.
35 L. Tai, C. Liu, K. Jiang, X. Chen, G. Wei, W. Lu and W. Pan, *Nanomedicine*, 2017, **13**, 2091–2100.
36 C. Liu, K. Jiang, L. Tai, Y. Liu, G. Wei, W. Lu and W. Pan, *ACS Appl. Mater. Interfaces*, 2016, **8**, 19256–19267.
37 Y. Qin, Y. Tian, Y. Liu, D. Li, H. Zhang, Y. Yang, J. Qi, H. Wang and L. Gan, *J. Pharm. Pharmacol.*, 2018, **70**, 1139–1151.
38 P. S. Apaolaza, M. Busch, E. Asin-Prieto, K. Peynshaert, R. Rathod, K. Remaut, N. Dunker and A. Gopferich, *Exp. Eye Res.*, 2020, **198**, 108151.
39 N. Kwak, N. Okamoto, J. M. Wood and P. A. Campochiaro, *Invest. Ophthalmol. Visual Sci.*, 2000, **41**, 3158–3164.
40 S. Zhao, R. Tian, B. Shao, Y. Feng, S. Yuan, L. Dong, L. Zhang, K. Liu, Z. Wang and H. You, *ACS Appl. Mater. Interfaces*, 2019, **11**, 394–402.
41 C. Yao, P. Wang, X. Li, X. Hu, J. Hou, L. Wang and F. Zhang, *Adv. Mater.*, 2016, **28**, 9341–9348.
42 H. Yang, P. Tyagi, R. S. Kadam, C. A. Holden and U. B. Kompella, *ACS Nano*, 2012, **6**, 7596–7606.
43 B. Liu, Y. Chen, C. Li, F. He, Z. Hou, S. Huang, H. Zhu, X. Chen and J. Lin, *Adv. Funct. Mater.*, 2015, **25**, 4717–4729.
44 B. Chen, W. Dai, D. Mei, T. Liu, S. Li, B. He, B. He, L. Yuan, H. Zhang, X. Wang and Q. Zhang, *J. Controlled Release*, 2016, **241**, 68–80.
45 L. Wang, Y. Chang, Y. Feng, X. Li, Y. Cheng, H. Jian, X. Ma, R. Zheng, X. Wu, K. Xu and H. Zhang, *Nano Lett.*, 2019, **19**, 6800–6811.